AD-A164 084 UNSTEADY AERODYNAMICS OF AIRFOIL OSCILLATING IN AND OUT 1/1
OF DYNAMIC STALL (U) GEORGIA INST OF TECH ATLANTA
SCHOOL OF AEROSPACE ENGINEERING C M WANG ET AL 1985
UNCLASSIFIED ARO-19364 7-EG-RW DAAG29-82-K-0094 F/G 20/4 NL

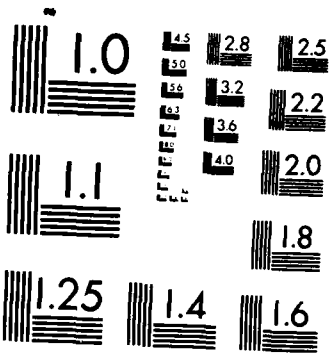

MASTER COPY FOR REPRODUCTION PURPOSES

UNCLASSIFIED
SECURITY CLASSIFICATION OF THIS PAGE (When Data Entered)

REPORT DOCUMENTATION PAGE

READ INSTRUCTIONS BEFORE COMPLETING FORM

1. REPORT NUMBER: ARO 19364.7-EG-RW
2. GOVT ACCESSION NO.: N/A
3. RECIPIENT'S CATALOG NUMBER: N/A

4. TITLE (and Subtitle): Unsteady Aerodynamics of Airfoils Oscillating In and Out of Dynamic Stall
5. TYPE OF REPORT & PERIOD COVERED: Reprint
6. PERFORMING ORG. REPORT NUMBER:

7. AUTHOR(s): C.M. Wang J.C. Wu and N.L. Sankar
8. CONTRACT OR GRANT NUMBER(s): DAAG29-82-K-0094

9. PERFORMING ORGANIZATION NAME AND ADDRESS: School of Aerospace Engineering, Georgia Institute of Technology
10. PROGRAM ELEMENT, PROJECT, TASK AREA & WORK UNIT NUMBERS:

11. CONTROLLING OFFICE NAME AND ADDRESS: U. S. Army Research Office, Post Office Box 12211, Research Triangle Park, NC 27709
12. REPORT DATE:
13. NUMBER OF PAGES:

14. MONITORING AGENCY NAME & ADDRESS (if different from Controlling Office):
15. SECURITY CLASS. (of this report): Unclassified
15a. DECLASSIFICATION/DOWNGRADING SCHEDULE:

16. DISTRIBUTION STATEMENT (of this Report): Approved for public release; distribution unlimited.

DTIC ELECTE FEB 11 1986 S D E

17. DISTRIBUTION STATEMENT (of the abstract entered in Block 20, if different from Report): NA

18. SUPPLEMENTARY NOTES: The view, opinions, and/or findings contained in this report are those of the author(s) and should not be construed as an official Department of the Army position, policy, or decision, unless so designated by other documentation.

19. KEY WORDS (Continue on reverse side if necessary and identify by block number): Aerodynamics, Dynamic Stall, Helicopters

20. ABSTRACT (Continue on reverse side if necessary and identify by block number): A solution procedure is presented for the computation of dynamic stall phenomena encountered by arbitrary shaped airfoils under arbitrary flow conditions. This procedure solves the unsteady, incompressible Navier-Stokes and the unsteady boundary layer equations using an efficient, zonal approach. A number of results for a modified NACA 0012 airfoil experiencing dynamic stall are presented and compared with available numerical data. Qualitative comparisons with flow visualization experiments are also presented.

DD FORM 1 JAN 73 1473 EDITION OF 1 NOV 65 IS OBSOLETE

UNCLASSIFIED
SECURITY CLASSIFICATION OF THIS PAGE (When Data Entered)

P-19364

AIAA'85

85-4078

UNSTEADY AERODYNAMICS OF AIRFOILS OSCILLATING IN AND OUT OF DYNAMIC STALL

C.M. WANG, J.C. WU AND L.N. SANKAR
Georgia Institute of Technology
Atlanta, GA 30332

AIAA 3rd Applied Aerodynamics Conference

October 14-16, 1985
Colorado Springs, Colorado

UNSTEADY AERODYNAMICS OF AIRFOILS OSCILLATING IN AND OUT OF DYNAMIC STALL

C.M. Wang*, J.C. Wu** and L.N. Sankar†
Georgia Institute of Technology
Atlanta, GA 30332

ABSTRACT

A solution procedure is presented for the computation of dynamic stall phenomena encountered by arbitrary shaped airfoils under arbitrary flow conditions. This procedure solves the unsteady, incompressible Navier-Stokes and the unsteady boundary layer equations using an efficient, zonal approach. A number of results for a modified NACA 0012 airfoil experiencing dynamic stall are presented and compared with available numerical data. Qualitative comparisons with flow visualization experiments are also presented. The present study also illustrates the effect of numerical viscosity on the accuracy and robustness of the solution procedure.

INTRODUCTION

The problem of dynamic stall is an important area of research in the helicopter industry, because of the large load variations, particularly the pitching moment variations, that occur during this phenomenon. Presently, the numerical modeling of this phenomenon is done primarily through a synthesis of existing dynamic stall experimental data . This approach is highly empirical in nature. It also relies on the availability of a large body of experimental data covering a wide range of airfoil shapes and flow conditions.

One of the earliest attempts to numerically simulate the dynamic stall phenomenon was made by Mehta (Ref. 1). In this work the incompressible, laminar Navier-Stokes equations were solved in the vorticity-stream function form using a finite difference solution procedure. This approach was able to predict the major features of the dynamic stall phenomenon, including the formation and shedding of a strong leading edge vortex. The laminar, compressible Navier-Stokes equations were used to compute the dynamic stall by Sankar and Tassa (Ref. 2). The effect of turbulence was accounted for in the works of Shamroth (Ref. 3) and Sankar and Tang (Ref. 4). The above approaches are all based on the finite difference solution of the governing equations and require large amounts of computer time and memory resources to accurately predict the dynamic stall phenomenon.

In the present work, a zonal solution procedure is used to perform dynamic stall calculations. This approach was previously developed for stationary airfoils of arbitrary shape experiencing massively separated flows (Ref. 5). Recently a number of improvements have been made to this approach to reduce the number of grid points and the computer time required to predict separated flows (Ref. 6).The present work addresses the extension of the algorithms and concepts implemented in References 5 and 6 to moving grids, and oscillating airfoils. Such an extension has resulted in a robust, useful solver capable of generating the dynamic stall load hysteresis loops in less than 30 minutes on a scalar machine such as the CDC CYBER 855 system.

The zonal approach used in this study was motivated by a number of factors. In many static and dynamic stall problems, the separated flow is confined to one of the airfoil surfaces (upper or lower) and the wake. On the other surface the flow is attached, and may be approximated by an unsteady boundary layer flow. The zonal approach presented here solves the computationally costly Navier-Stokes equations only in the separated regions. On the attached flow side, the boundary layer equations are solved. This reduces the number of points where the Navier-Stokes equations are solved by approximately a factor of two. Secondly, since in the separated flow regions the length scales of the vortices of interest are large compared to the length scales in the boundary layer regions, a coarser grid may be used in the separated region. This also translates into fewer points and larger time steps in the separated regions.

A second feature of the present zonal approach is the ability to bring the far field boundaries closer to the airfoil. This is achieved by a closed form specification of the velocities and/or stream function values on the far field boundary using the Biot-Savart law. The use of smaller computational domains allow the grid points to be packed close to the solid surface, and also allows the grid to stretch smoothly from the airfoil surface to the far field. This is an important consideration in numerical solutions if second order spatial accuracy is to be guaranteed.

The zonal approach uses an integral form of the kinematic equations to determine the velocity and stream function values in the

---

* Post Doctoral Fellow, Member AIAA
** Professor, Associate Fellow AIAA
† Associate Professor, Member AIAA

separated regions, thus removing the need to obtain the numerical solution of the Poisson's equation for the stream function iteratively. In the past, integral approaches such as the one employed here were not as efficient as expected because of the need to repeatedly compute or store the geometric influence coefficients. In the present work, a Fourier series expansion of the vorticity field along one of the coordinate directions is used to simplify the evaluation of the velocities.

Another important feature of the present zonal approach is the procedure for the determination of the surface vorticity, generated at each time step to satisfy the no slip conditions. The procedure described here ensures that the global conservation of vorticity is satisfied. This procedure allows the surface vorticity distribution to be determined with good accuracy, and also permits the distribution of surface pressures which depend on the vorticity gradient at the surface, to be calculated accurately.

In the following sections, the governing equations and the numerical procedure are described. In a separate section, the computer time and memory requirements are given. Finally, a number of numerical results are presented for the dynamic stall phenomenon experienced by a modified NACA 0012 airfoil, and compared with available numerical data and flow visualization studies.

MATHEMATICAL FORMULATION

Governing Equations:

In order to handle arbitrary airfoils undergoing arbitrary motion, a body-fitted, orthogonal O-grid system is first constructed. In the present work, the above coordinate system was constructed through an analytical or numerical conformal mapping of the airfoil shape onto a unit circle, followed by a distribution of nodes on the exterior of the unit circle. This distribution is such that a sufficiently large number of nodes are clustered in the vicinity of the airfoil. The (r, θ) circle plane used in this work is referred to as the ζ- plane. The physical plane (x,y) is referred to as the z- plane.

The governing equations for the unsteady incompressible viscous flow past a rotating airfoil take the following form in the circle plane :

$$\nabla \times \bar{\psi} = \bar{v}$$

$$\nabla \times \bar{v} = - \omega H^2 \bar{k}$$

$$H^2 \omega_t + (\nabla \times \bar{\psi}') \cdot \nabla\omega = \nu \nabla^2 \omega \qquad (1)$$

In the above equations, H is the scale factor of transformation given by

$$H^2 = (x_r y_\theta - x_\theta y_r)/r \qquad (2)$$

This quantity may be determined analytically if the conformal mapping is a Joukowski transformation. It may be numerically determined otherwise. The quantity ψ' is the stream function in the rotating frame of reference, and is related to the stream function ψ in a stationary frame of reference through the following relationship:

$$\psi' = \psi + \Omega(x^2 + y^2)/2 \qquad (3)$$

Finally, ω is the vorticity distribution, as observed in an inertial frame of reference, and Ω is the angular velocity of the airfoil.

Boundary Layer Approximation:

In the applications considered here, the viscous flow region over the lower surface is confined to a very thin boundary layer. Favorable pressure gradients exist over most of the entire lower surface. For this reason, in the present application, the streamwise diffusion terms appearing in the vorticity transport equation were neglected, giving the following unsteady, parabolic partial differential equation for ω:

$$H^2 \omega_t + (\nabla \times \bar{\psi}') \cdot \nabla\omega = \nu \left(\frac{\partial^2 \omega}{\partial y^2} + \frac{1}{r} \frac{\partial \omega}{\partial r} \right) \qquad (4)$$

The above assumption allows the vorticity field in the boundary layer region to be determined using a simple non-iterative marching scheme, starting from the leading edge stagnation point.

Integral Formulation of the Kinematics:

The kinematic relationships for the stream function may be reexpressed as an integral expression for the velocity field in the circle plane. If this is done, the following integral equation results:

$$\nabla \times \bar{\psi} = \frac{1}{2\pi} \iint \frac{\omega H^2 \bar{k} \times (\bar{r} - \bar{r}_o)}{|\bar{r} - \bar{r}_o|^2} r_o dr_o d\theta_o +$$

$$\frac{1}{2\pi} \oint \frac{(\nabla \times \bar{\psi}) \cdot \bar{n}_o (\bar{r} - \bar{r}_o) - (\nabla \times \bar{\psi}) \times (\bar{n}_o) \times (\bar{r} - \bar{r}_o)}{|\bar{r} - \bar{r}_o|^2} r_o d\theta_o \qquad (5)$$

In the above equation, $\bar{r}$ is the position vector of the point where the velocity is computed. Also, r_o is the variable of integration. The term $\oint$ contains the contributions of the freestream. The line integral over the unit circle is zero for

stationary airfoils, but is a non-zero quantity for oscillating airfoils. The term n_o appearing in the above line integral is an outward pointing unit vector.

Integral Formulation for the Surface Vorticity:

The surface vorticity generated at every time step should satisfy the zero normal and tangential velocity conditions. The law of conservation of vorticity should also be satisfied. In the present application, the integral relationship for the velocity at the interior points may be used directly to determine the surface voriticity distribution. The details of the surface vorticity determination are given in the following section.

NUMERICAL FORMULATION

Discretization of the Integral Equation for Velocity:

In order to evaluate the velocity field V at any point in the computational field, the following strategy was used. The grid generated using the mapping procedure may be thought of as a collection of cells. Inside every cell the vorticity value is considered invariant in the radial direction. In the θ-direction, it was assumed that the vorticity field may be approximated by the following finite Fourier series:

$$\omega(r, \theta)H^2 = \frac{\alpha_o(r)}{2} + \sum_{n=1}^{N} [\alpha_n(r)\cos n\theta + \beta_n \sin n\theta] \qquad (6)$$

The two components of the velocity vector were also expressed as the following Fourier Series expansions :

$$V_r = \frac{a_o(r)}{2} + \sum_{n=1}^{N} [a_n(r)\sin n\theta + b_n(r)\cos n\theta] \qquad (7)$$

$$V_\theta = \frac{c_o(r)}{2} + \sum_{n=1}^{N} [c_n(r)\sin n\theta + d_n(r)\cos n\theta]$$

When the above series expansions are substituted into Equation (5), the resulting expressions may be analytically integrated both in the θ- and the radial directions. This yields a simple, recursive relationship between the coefficients of the series for the vorticity, and the coefficients of the series for the velocity field. For example, on all node points located on a circle given by r= constant, one obtains,

$$c_o(r) = \int_1^r \alpha_o \frac{r_o}{r} dr_o + c_o(1)/r \qquad (8)$$

For a complete list of the recursive relationships between the various Fourier coefficients, the reader is referred to Reference 7.

Once, the coefficients of the Fourier series expansions are determined, the velocity values at any point in the flow field may be found. In the present work, this discretization was used at all the nodes in the computational domain where velocity values are needed, including the nodes within the boundary layer region.

Determination of Surface Vorticity:

The surface vorticity values which are needed at every time step were obtained as follows. The integral equation for the velocity is applied at the airfoil surface, given by r=1 in the circle plane:

$$\frac{1}{2\pi}\iint \frac{\omega_o H_o^2 \bar{k} \times (\bar{r} - \bar{r}_o)}{|\bar{r} - \bar{r}_o|^2} r_o dr_o d\theta_o = I(r) \qquad (9)$$

The right hand side of the above equations is the contribution due to the velocity of the fluid at the airfoil surface in the transformed plane, and is entirely due to the rotation of the airfoil about a pitching axis.

The Fourier series expansions for the vorticity field are now substituted into the above equation. The right hand side of this equation is also expressed as a finite Fourier series expansion. All the terms which are multiples of the same sine or cosine term are then grouped together, and each group of terms is individually set to zero. If the above procedure is followed, then 2N equations result for the 2N+1 coefficients of the Fourier series for the vorticity distribution at the airfoil boundary. The additional equation required to determine all the 2N+1 coefficients uniquely is the law of total conservation of vorticity, given by:

$$\iint \omega_o H^2 r_o dr_o d\theta_o + 2\Omega A = 0 \qquad (10)$$

Where A is the area enclosed by the airfoil in the physical plane. This approach gives an explicit relationship for the Fourier coefficients for the vorticity distribution at the airfoil, in terms of the vorticity field away from the airfoil surface. Note that this approach is consistent with the way the interior velocity components are

evaluated, and avoids any non-unique specification of the surface vorticity. For a set of explicit relationships between the Fourier coefficients of the surface vorticity and the interior vorticity, the reader is referred to Ref. 7.

Numerical Treatment of the Vorticity Transport Equation:

In the separated flow regions, the vorticity transport equation was discretized as follows:

$$H^2 \bar{\delta}_\tau \omega + \frac{1}{r} \delta_r \psi \bar{\delta}_\theta \omega - \frac{1}{r} \delta_\theta \psi \bar{\delta}_r \omega = \nu [\delta_{rr} + \frac{1}{r} \delta_r + \frac{1}{r^2} \delta_{\theta\theta}] \omega \qquad (11)$$

In the above discretization, δ_θ , δ_r etc. are the standard central differences which take into account the fact that the grid is not uniformly spaced in the radial direction. The quantity $\bar{\delta}_\tau$ is the backward difference operator with respect to time. The operators $\bar{\delta}_\theta$ and $\bar{\delta}_r$ are four-point upwind difference operators, patterned after the QUICK upwind scheme proposed by Leonard (Ref. 8).

All the vorticity values appearing in the upwind differences and the viscous terms were kept at the unknown time level. Thus the vorticity values at all the nodes are coupled to each other in a fully implicit manner. These vorticity values were iteratively solved for, using a successive line under relaxation point scheme. The values of the vorticity at the boundary were also updated simultaneously with the interior vorticity values.

In the boundary layer regions, the same discretization was used, except the diffusion terms along the θ-direction were suppressed. Since the flow velocities relative to the grid are always from the leading edge to the trailing edge on the lower surface for the low reduced frequencies considered here, the vorticity transport equation in the boundary layer region may be solved using a simple marching scheme. Since the boundary voriticty values in the boundary layer region are coupled strongly to the vorticity values in the separated region, these values change from one iteration to another. Thus, it is necessary to solve the boundary layer equations iteratively, along with the vorticity transport equation in the separated flow region.

All the calculations were carried out by starting the flow from rest implusively, and marching in time until a steady state or a periodic solution is achieved. In the case of the dynamic stall calculations, a steady solution was first obtained at the lowest angle of attack experienced by the airfoil during the dynamic stall. This steady state solution was used as the initial condition for the oscillating airfoil problem.

When advancing the solution from one time step to the next, the following procedure is followed:

1. The velocity values at all the interior nodes are computed using the Fourier Series expansion approach discussed earlier. The velocity values at the far field boundary were also updated. The contributions of any vorticity that had left the computational domain through convection was negelected in this step.

2. The vorticity values at the interior were updated (both the separated and the boundary layer region) to get a first estimate of the vorticity field at the new time level. This value was under-relaxed by an user input under relaxation factor.

3. The vorticity values at the solid surface were updated, to be consistent with the interior vorticity values.

Steps 2 and 3 are repeated a number of times until the vorticity values at all the interior nodes and boundary nodes are fully converged.

For additional details of the solution procedure, and its application to separated flow problems, the reader is referred to References 5 and 6.

RESULTS AND DISCUSSION

All the calculations presented here are for a modified NACA 0012 airfoil. This airfoil was chosen, because some well documented numerical results for the laminar dynamic stall phenomenon, and some water tunnel flow visualization studies are available for this airfoil (Ref. 1,9). This airfoil may be mapped onto a unit circle using the following Joukowski transformation:

$$z = \zeta + \gamma + \frac{C}{\zeta + \gamma}$$

Here $z = x + i\,y$, and $\zeta = r \exp(-i\theta)$. The constants C, γ etc. determine the type of the resulting airfoil shape. By a careful selection of these coefficients, the airfoil thickness, its camberline shape, leading and trailing edge radii etc. may be controlled.

The airfoil surface was represented by 50 nodes in the computations, clustered near the leading and the trailing edge for maximum accuracy. In the radial direction 60 nodes were located. The stretching in the radial direction was such that a minimum of 15 nodes were located within the boundary layer on the lower surface. The location of the first point of the wall in the circle plane was typically between 0.006 and 0.003 units.

All the oscillating airfoil calculations were done about a mean angle of attack of 10 degrees, and an amplitude of oscillation equal to 10 degrees.The following cases were considered:

1. Reynolds Number 5000, Reduced Frequency based on chord equal to 0.25.

2. Reynolds number 10000, 0.25 reduced frequency.

3. Reynolds Number 1000, 0.25 reduced frequency

4. Reynolds number 5000, 0.5 reduced frequency

A steady state solution at zero angle of attack was supplied as the initial condition in all the dynamic stall calculations.

In Figures 1 and 2 the constant vorticity contours and streamlines in the rotating coordinate system are shown for case 1. In Figure 3, the integrated airfoil loads are also shown.These figures reveal the slow forward progression of the separation point on the upper surface as the airfoil pitches up. A large amount of counterclockwise (positive) vorticity is being shed into the wake during this phase of the upstroke, upto 18 degrees airfoil incidence. The separated region remains confined to a narrow region on the upper surface. The airfoil lift continues to grow during this phase of the upstroke as shown in Figure 3.

Between 18 and 19 degrees during the upstroke, the shedding of the positive vorticity into the wake stops, and a region of counterclockewise vorticity begins to grow on the upper surface as seen in Figures 1b and 2c. The airfoil lift coefficient experiences a momentary drop as shown in Figure 3a.

Subsequently, a leading edge vortex of clockwise sense begins to grow near the quarter chord as shown in Figure 1b. The strength of the vortex increases with the airfoil incidence. The lift coefficient begins to grow, but the moment coefficient remains relatively unaffected. This is because the pressure suction peaks associated with the vortex are too close to the moment axis (quarter chord) to influence the moment coefficient.

As the leading edge vortex grows in strength it begins to drift downstream, at a speed equal to approximatley half the freestream velocity. The lift coefficient continues to grow as shown in portion BC of the lift curve in Figure 3a. The moment coefficient begins to increase in magnitude because the suction peaks associated with the vortex are now sufficiently far away from the pitching axis, and eventually moment stall occurs, as shown in portion BC in Figure 3b. The lift stall occurs when the vortex reaches the airfoil trailing edge as shown in Figures 2e and 2f and in the lift curve (Figure 3a). The pitching moment recovers however, as the lift drops, as seen in Figure 3b.

During the downstroke, the flow on the airfoil gradually reattaches from the leading edge to the trailing edge. The laminar flow on the airfoil is unable to withstand the relatively small adverse pressure gradients that exist during this phase of the flow, and a sequence of small vortices of positive and negative strength are shed into the wake. This accounts for the large oscillations in the lift and moment forces shown in Figures 3a and 3b. This is in contrast to turbulent flows (Ref. 3, 4) where similar variations are not observed during the downstroke.

The drag variations during the dynamic stall process are shown in Figure 3c. Except at small angles of attack, the primary contribution to the drag is from the pressure drag.

Some numerical experiments were done to determine the effect of numerical viscosity due to the upwind differencing of the convection terms, on the solution. In Figure 4, the load hysteresis for case 1, computed with a first order accurate upwind difference scheme is shown. The large numerical viscosity associated with the first order scheme smears out a number of features observed using the third order accurate upwind scheme, and only a qualitative resemblance between Figures 3 and 4 is found.

Case 2, is similar to case 1 except the flow Reynolds number is increased from 5000 to 10000. In Figure 5 the lift and moment hysteresis loops are shown for case 2.

Case 3 is similar to cases 1 and 2 except the Reynolds number was 1000. At this lower Reynolds number no clearly distinguishable leading edge vortex structure was observed, as seen in the streamline contours (Figure 6). The associated lift and moment loops are plotted in Figure 7.

This type of dynamic stall is often classified as the trailing edge stall.

The last set of dynamic stall calculations presented here are for the same flow conditions as case 1, except at the slightly higher reduced frequency of 0.5. This case was chosen because of the availability of numerical data (Ref. 1) and water tunnel flow visualization pictures. The physical phenomena at this reduced frequency are very similar to case 1. The actual drop in lift and moment coefficients are however smaller than at the lower reduced frequency. In Figure 8, the lift, drag and moment hysteresis loops are plotted and compared with the results of Mehta. Good quantitative agreement is observed during the upstroke, but some discrepancies between the two set of data is found during the downstroke. In view of the differences in the solution procedures used in Reference 1 and in this work, these differences are not unreasonable. In Figure

9, the streamlines in an inertial frame are plotted at selected time levels and compared with the water tunnel observations of Werle' presented in Reference 1. Excellent agreement between these two sets of data is found.

In all the cases computed above, computer time per case ranged between 15 and 30 minutes on a CDC CYBER 855, depending on the reduced frequency and Reynolds number. This code is now being vectorized for a CDC CYBER 205 computer system, and preliminary calculations show that the computer time per cycle can be reduced to less than 2 minutes on this system.

CONCLUDING REMARKS

An efficient solution procedure has been developed for the prediction of the dynamic stall characteristics of arbitrary airfoils in laminar, incompressible flow. This solution procedure is an order of magnitude more efficient than existing finite difference procedures for the same problem. A two layer eddy viscosity model is being implemented into this solver and will be used to study turbulent dynamic stall.

The computations reveal characteristics similar to turbulent leading edge stall at Reynolds numbers 5000 and 10000, while at the lower Reynolds number of 1000, a trailing edge stall phenomenon is observed. The effect of higher reduced frequencies is to reduce the lift and moment drops when stall occurs.

ACKNOWLEDGEMENTS

This work was supported by the U.S. Army Research Office under the Center of Excellence in Rotary Wing Aircraft Technology (CERWAT) program.

REFERENCES

1. Mehta, U.B., "Dynamic Stall of an Oscillating Airfoil," Proceedings of the AGARD Conference on Unsteady Aerodynamics, AGARD CP-227, September 1977.

2. Sankar, L.N., "Reynolds Number and Compressibility Effects on the Dynamic Stall of a NACA 0012 Airfoil," AIAA Paper 80-0010.

3. Shamroth, S.J., "Calculations of Oscillating Airfoil Flowfield via the Navier-Stokes Equations," AFOSR/FLSRL/University of Colorado Workshop on Unsteady Separated Flow, August 10-11, 1983.

4. Sankar, L.N. and Tang, W., "Numerical Solution of Unsteady Viscous Flow past Rotor Sections," AIAA Paper 85-0129.

5. Wu, J.C. and Gulcat, U., "Separate Treatment of Attached and Detached Flow Regions in General Viscous Flows," AIAA Journal, Vol. 19, No. 1, pp 20-27, 1981.

6. Wu, J.C., Wang, C.M. and Gulcat, U., "Zonal Solution of Unsteady Viscous Flow Problems," AIAA Paper 84-1637.

7. Wang, C.M. and Wu, J.C., "Numerical Solution of Navier-Stokes Problems Using Integral Representations with Series Expansions," AIAA Paper 85-0034.

8. Leonard, B.P., "A Stable and Accurate Convective Modeling Procedure on Quadratic Upstream Interpolation," Computer Methods in Applied Mechanics and Engineering, Vol. 19, 1979, pp 59-98.

(a) Angle of Attack = 16.90°

(b) Angle of Attack = 18.34°

(c) Angle of Attack = 19.84°

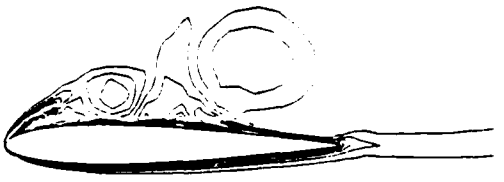

(d) Angle of Attack = 19.53.

Figure 1. Vorticity Contours around an Oscillating NACA 0012 Airfoil. Reynolds Number 5000, 0.25 Reduced Frequency.

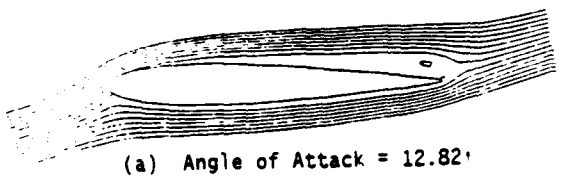

(a) Angle of Attack = 12.82°

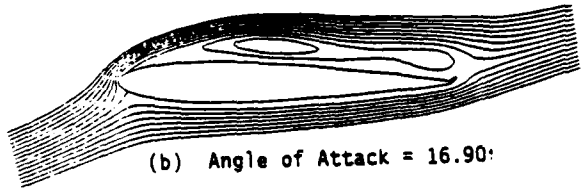

(b) Angle of Attack = 16.90°

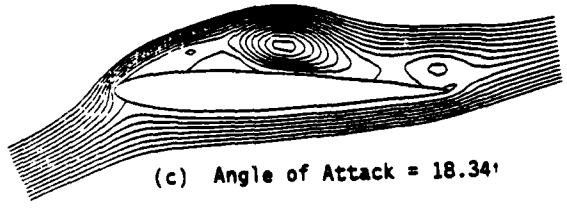

(c) Angle of Attack = 18.34°

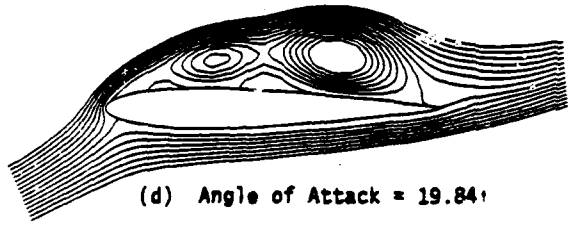

(d) Angle of Attack = 19.84°

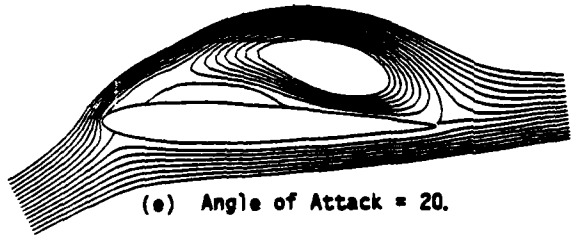

(e) Angle of Attack = 20.

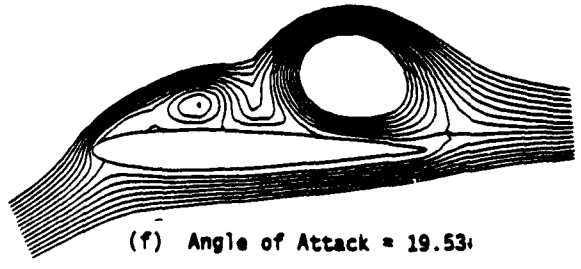

(f) Angle of Attack = 19.53°

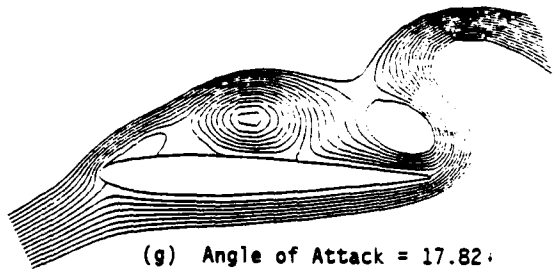

(g) Angle of Attack = 17.82°

Figure 2. Streamlines in the Rotating Frame around an Oscillating NACA 0012 Airfoil. Reynolds Number 5000, 0.25 Reduced Frequency.

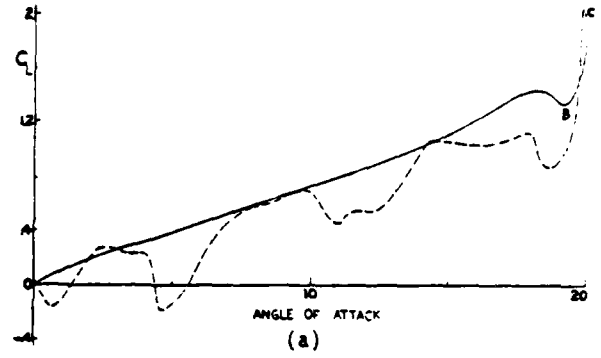

(a)

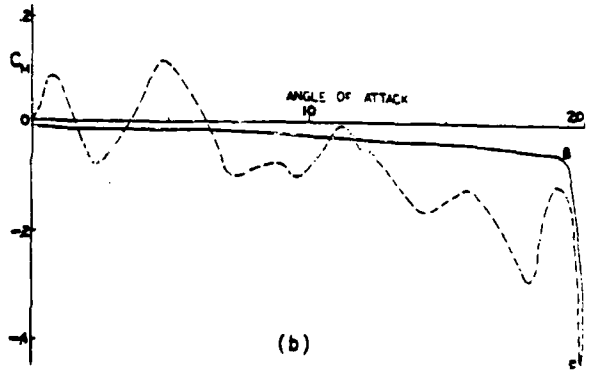

(b)

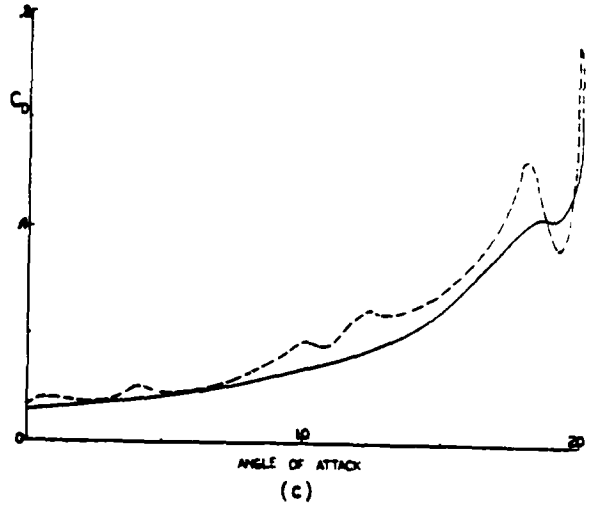

(c)

Figure 3. Lift, Moment and Drag Hysteresis Loops for a NACA 0012 Airfoil. Reynolds Number 5000, 0.25 Reduced Frequency.

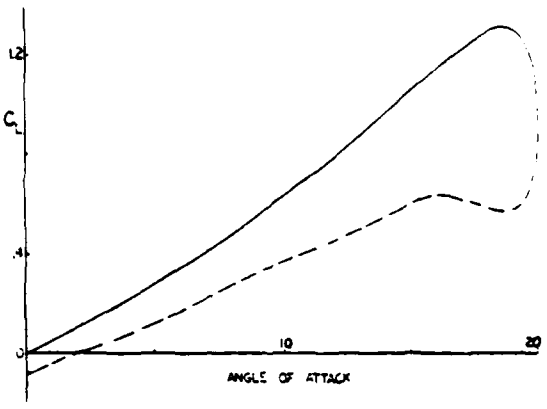

Figure 4. Lift Hysteresis Loop computed Using a First Order Upwind Scheme. NACA 0012 Airfoil, Reynolds Number 5000, 0.25 Reduced Frequency.

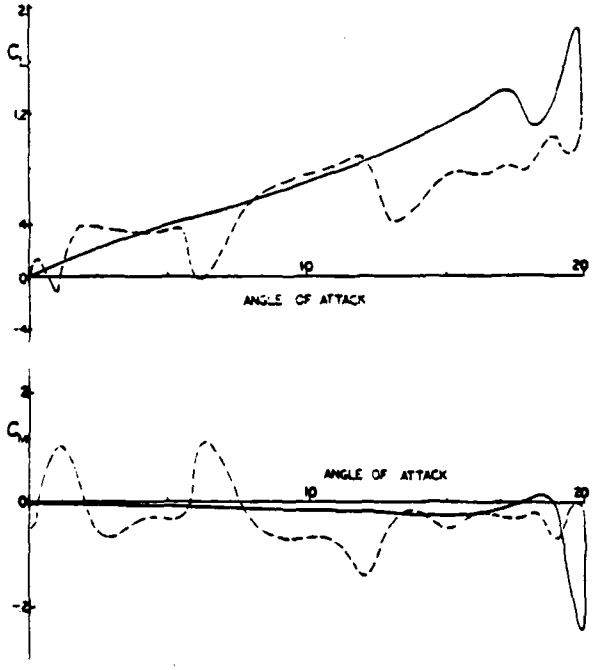

Figure 5. Lift and Moment Hysteresis Loops at Reynolds Number 10000, 0.25 Reduced Frequency.

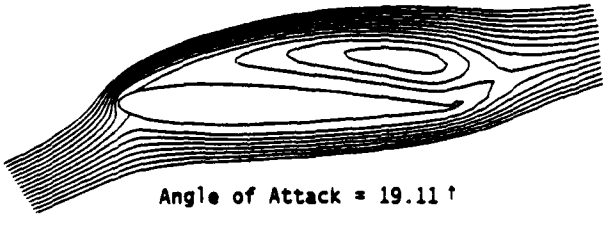

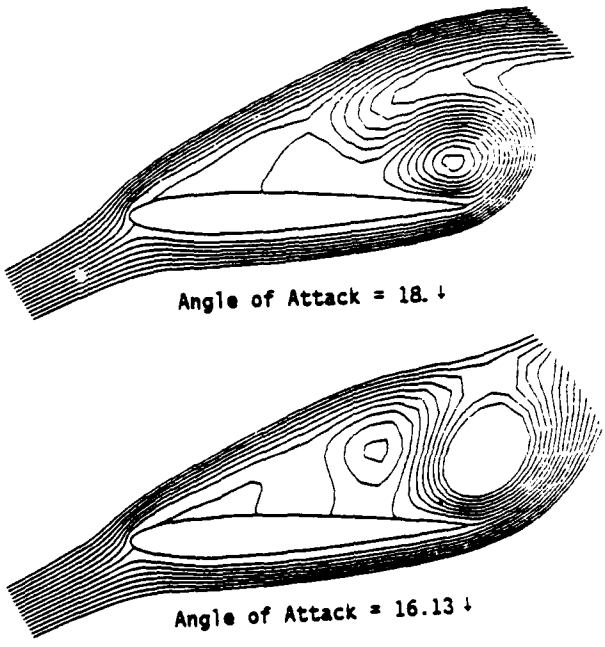

Figure 6. Streamlines in the Rotating Frame around an Oscillating Airfoil. Reynolds Number 1000, 0.25 Reduced Frequency.

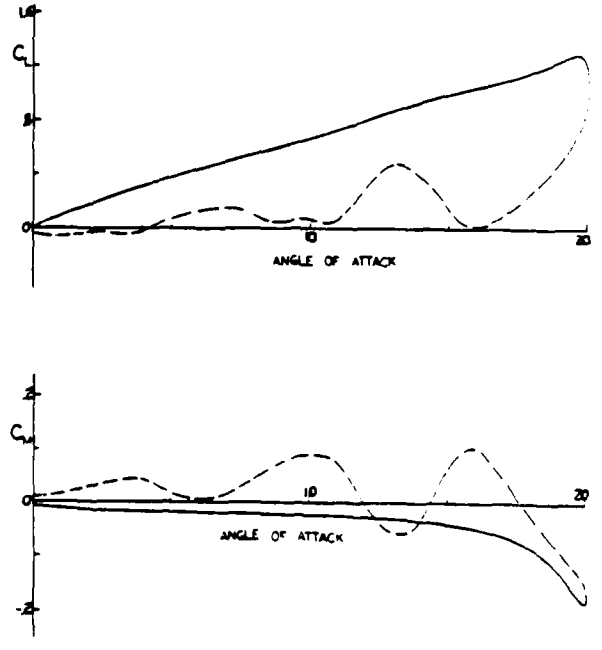

Figure 7. Lift and Moment Hysteresis Loops for a NACA 0012 Airfoil. Reynolds Number 1000, 0.25 Reduced Frequency.

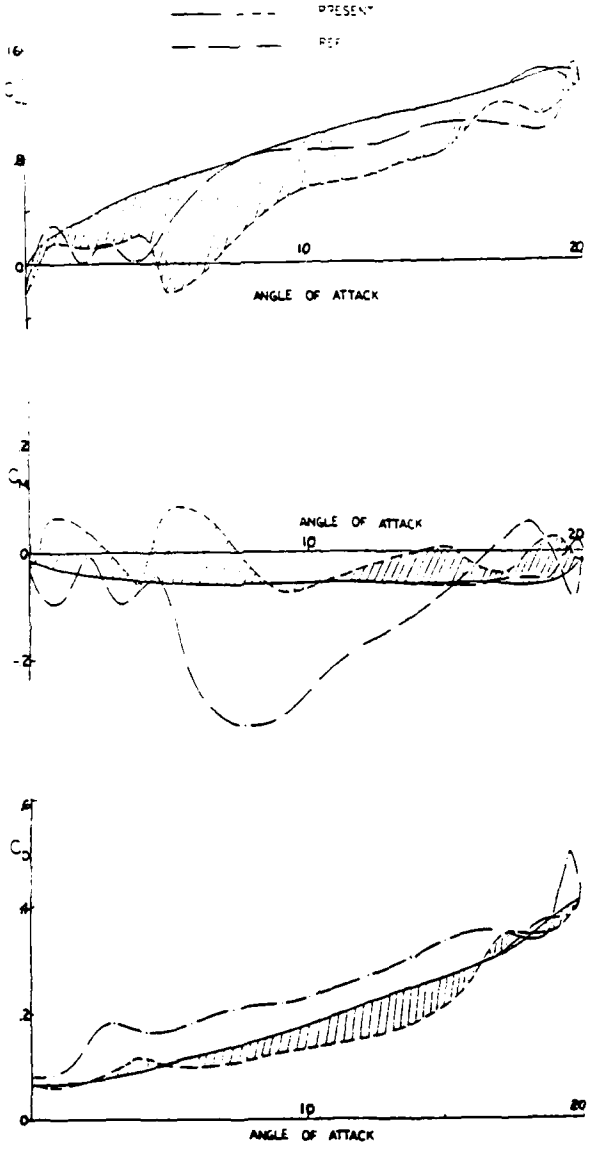

Figure 8. Comparison of Lift and Moment Hysteresis Loops Computed Using the Present Scheme with the Results of Mehta. Reynolds Number 5000, 0.5 Reduced Frequency.

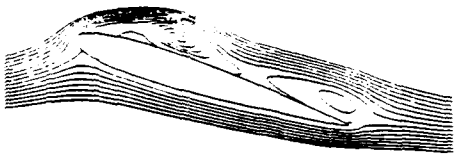

Angle of Attack = 20.

Figure 9. Comparison of Streamline in the Inertial Frame with Water Tunnel Observations. Reynolds Number 5000, 0.5 Reduced Frequency.

END

FILMED

3 -86

DTIC